Ultra-Fast Tunable Optical Delay Line Based on Cascaded Silicon Microdisk Resonators

Yuwen Xu, Weifeng Zhang, *Member, IEEE*, and Bin Wang, *Member, IEEE*

***Abstract*—Integrated optical delay lines (ODLs) featuring fast and continuous tunability are important building blocks in microwave photonic signal processing systems. In this work, we propose and demonstrate an ultra-fast tunable ODL based on cascaded silicon microdisk resonators (MDRs). In the proposed integrated ODL, a specially designed MDR is used as the basic delay element, which has an additional slab waveguide to surround the disk and the bus waveguide aiming to suppress higher-order whispering gallery modes (WGMs) and to support the incorporation of a lateral PN junction for electrical tunability. By exploiting the free-carrier dispersion (FCD) effect on silicon, the proposed ODL can be tuned with an ultrahigh speed. Multiple MDRs are connected in series to increase the time delay provided by the ODL. As a demonstration, integrated ODLs with 5 and 10 MDRs are designed and fabricated. The experimental results show that the fabricated ODL provides an ultra-short response time of 989 ps, a low power consumption below 0.58 mW, and a small footprint of 0.13 mm^2. The proposed integrated ODL holds great advantages including ultra-high tuning speed, low power consumption and ultra-compact footprint, which is potential to be widely used in next-generation phased array radar and high-speed wireless communication systems.**

***Index Terms*—Microdisk resonator, optical delay line, ultrahigh tuning speed.**

I. Introduction

OPTICAL delay line (ODL) is one of the key components in microwave photonic processing systems [1], [2], [3], [4], [5]. Especially, ODL-based beamforming networks are widely used to perform beam steering with a wide operational bandwidth and a high scanning speed [6], [7]. Up to date, most of the commercially available ODLs are realized based on discrete free-space or fiber-optic components, which suffer from a high cost, a large size, a high power consumption and a long response time. To address these problems, integrated ODL fabricated on silicon on insulator (SOI) platform is a promising solution [8], [9], [10], [11], which holds unique advantages of high tuning speed, small footprint, and CMOS compatibility.

In the last few years, numerous silicon integrated ODLs have been demonstrated based on different configurations, such as switchable waveguide delay lines (SWDLs) [12], [13], [14], [15], [16], [17], waveguide Bragg gratings [18], [19], [20], [21], [22], [23], microring resonators (MRRs) [24], [25], [26], [27], [28], [29], [30], [31], microdisk resonators (MDRs) [32], [33], [34], and photonic crystal waveguides (PhCW) [35], [36]. Among them, ODLs based on MRRs or MDRs have attracted intensive attention due to their unique advantages including large group delay, high tuning efficiency, and compact footprint. Previously, an ODL based 56 cascaded MRRs has been demonstrated, which provides a large group delay exceeding 500 ps [24], but the time delay provided by the ODL cannot be flexibly tuned since it is fabricated on a passive chip without any tuning mechanism. In order to achieve continuous time delay tuning, ODLs based on thermally tunable MRRs have been proposed, in which a metal heater is placed on the top of the ring waveguides [26], [27], [28]. However, the tuning speed of this kind of ODL is at the level of tens of microseconds, which is limited by the slow response time of the thermal-optic (TO) effect on silicon. Moreover, the power consumption of thermally tunable ODLs is normally as high as a few tens of milliwatts, which hinders their applications in some fields where low power consumption is required. Alternately, electrically tunable ODLs with a high tuning speed and a low power consumption can also be realized based on an electrically tunable MRR, in which a PIN diode is incorporated in the MRR [30]. By exploiting the carrier injection effect, the ODL based on an electrically tunable MRR can achieve a high tuning speed and a low power consumption. Compared with the PIN diode, the PN junction structure is potential to achieve a much higher tuning speed by exploiting the carrier depletion effect on silicon, and high-speed optical devices such as silicon MRR modulators with a bandwidth as wide as a few tens of GHz have already been demonstrated [37]. However, ultra-fast tunable ODLs based on electrically tunable MRRs or MDRs with PN junctions are yet to be developed.

In this paper, we propose and demonstrate an ultra-fast tunable ODL based on cascaded silicon MDRs. Different from MRRs, MDRs experience scattering loss only from the outer sidewall of the waveguide, which leads to a better performance in terms of footprint and light-confining capacity. In the proposed integrated ODL, a specially designed MDR with a small radius of 3.7 μm is used as the basic delay element, which has an additional slab waveguide to surround the disk and the bus waveguide aiming

Manuscript received 20 June 2023; revised 21 July 2023; accepted 26 July 2023. Date of publication 7 August 2023; date of current version 18 August 2023. This work was supported in part by the National Key R&D Program of China under Grant 2018YFE0201800, in part by the National Natural Science Foundation of China under Grants 62105028, 62071042, and U22A2018, and in part by China Postdoctoral Science Foundation under Grant 2021M690390. *(Corresponding author: Bin Wang.)*

The authors are with the Radar Research Lab, School of Information and Electronics, Beijing institute of Technology, Beijing 100081, China, also with the Key Laboratory of Electronic and Information Technology in Satellite Navigation (Beijing institute of Technology), Ministry of Education, Beijing 100081, China, also with the Beijing institute of Technology Chongqing Innovation Center, Chongqing 401120, China, and also with the Chongqing Key Laboratory of Novel Civilian Radar, Chongqing 401120, China (e-mail: yuwen.xu@bit.edu.cn; weifeng.zhang@bit.edu.cn; bin.wang@bit.edu.cn).

Digital Object Identifier 10.1109/JPHOT.2023.3300898

This work is licensed under a Creative Commons Attribution 4.0 License. For more information, see https://creativecommons.org/licenses/by/4.0/

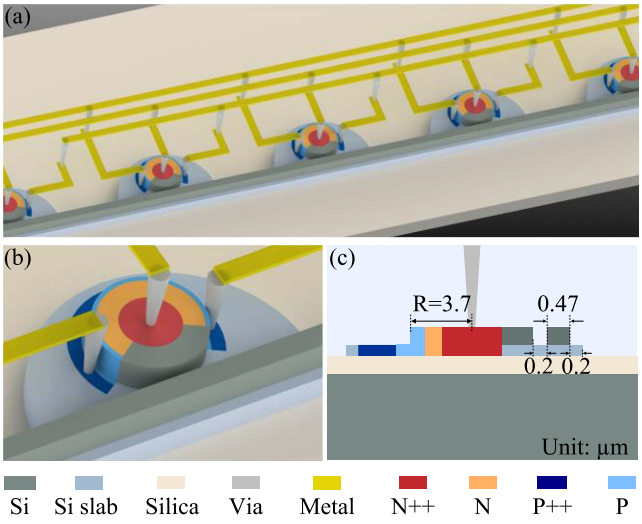

Fig. 1. (a) Perspective view of the proposed ODL. (b) Zoom-in view of the tunable MDR with PN junction. (c) Cross-sectional view of the MDR.

to suppress higher-order whispering gallery modes (WGMs) and to support the incorporation of a lateral PN junction for electrical tunability. By exploiting the free-carrier dispersion (FCD) effect on silicon, the proposed ODL can be tuned with an ultrahigh speed. Multiple MDRs are connected in series to increase the time delay provided by the proposed ODL. As a demonstration, integrated ODLs with 5 and 10 MDRs are designed and fabricated. The experimental results show that the fabricated ODL provides an ultra-short response time of 989 ps, a low power consumption of 0.58 mW, and a small footprint of 0.13 mm^2. The proposed integrated ODL holds great advantages including ultra-high tuning speed, low power consumption and ultra-compact footprint, which is promising to be widely used in next-generation phased array radar and high-speed wireless communication systems.

II. Device Design and Fabrication

Fig. 1(a) shows the perspective view of the proposed ultrafast tunable ODL. It consists of multiple identical MDRs which are connected serially to form an MDR array. Fig. 1(b) shows the zoom-in view of the MDR which has an all-pass configuration consisting a bus waveguide and a disk waveguide. The proposed MDR has an additional slab waveguide employed to wrap the disk and the lateral sides of bus waveguide, which is used to suppress the higher-order WGMs of the MDR and to support the incorporation of the lateral PN junction. The lateral PN junction of the disk is formed along the edge of the disk to achieve ultra-fast tuning of the proposed ODL, which is composed of N, N++, P and P++ doping regions. In order to minimize the absorption loss induced by heavy doping, the P++ and N++ implantation regions are placed 1 μm away from the center of the PN junction. To avoid the optical coupling region between the bus waveguide and the disk to be deteriorated, there is no doping region along the arc with an angle of 120° near the coupling region of the MDR. Fig. 1(c) shows the cross-section view of the MDR. The disk is designed to have an ultra-small radius of 3.7 μm and the slab waveguide has a radius of 9.5 μm. In order to meet the phase matching condition between the disk and the bus waveguide, the effective refractive index of the fundamental mode existed in the bus waveguide should be equal to that of the fundamental WGM existed in the disk waveguide. The bus waveguide is optimized to have a width of 470 nm. The coupling gap between the bus waveguide and the disk has a width of 200 nm. The disk and the slab waveguide of the MDR has a height of 220 nm and 90 nm, respectively.

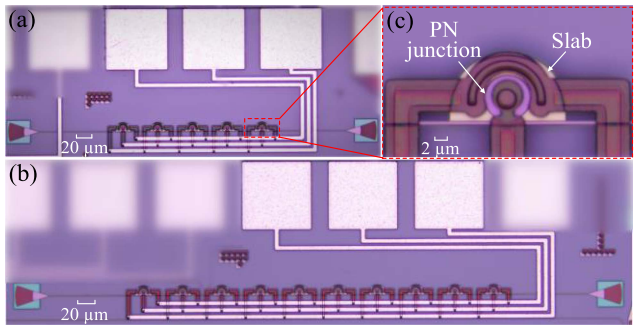

Fig. 2. Microscope images of the fabricated ODLs. (a) ODL consisting of 5 cascaded MDRs. (b) Zoom-in view of the fabricated MDR with PN junction. (c) ODL consisting of 10 cascaded MDRs.

The proposed device is fabricated using standard CMOS fabrication processes on a SOI wafer in IME. ODLs consisting of 5 MDRs and 10 MDRs are designed and fabricated. Fig. 2(a) and (b) show the microphotographs of the fabricated ODLs comprising 5 MDRs and 10 MDRs with metal wires and pads, respectively. Fig. 2(c) shows the zoom-in-view of the fabricated MDR. The fabricated ODL composed of 5 MDRs has a length of 480 μm and a width of 189 μm, giving a compact footprint of 0.09072 mm^2. The fabricated ODL composed of 10 MDRs has a length of 705 μm and a width of 185 μm, giving a total footprint of 0.13 mm^2.

III. Experimental Results

A. Delay Performance

The magnitude response and the delay performance of the fabricated ODLs are characterized using an optical vector analyzer (OVA). The OVA is realized based on a polarization-diverse swept-wavelength interferometry, which mainly consists of a frequency-swept laser, two Mach-Zehnder interferometers (MZIs), and a parameter extraction unit. The group delay value of the ODL can be obtained directly from the OVA [38]. Firstly, the performance of a single MDR which is used as the basic delay element is evaluated. Fig. 3(a) illustrates the normalized transmission spectrum of the MDR delay element. As can be seen, the disk supports only the fundamental WGM while the higher-order WGMs are suppressed effectively. The fiber-to-fiber I/O coupling loss is 18 dB, which can be further reduced by optimizing the structure of the grating coupler. The free spectrum range (FSR) of the MDR is measured to be 30.03 nm, which is determined by the radius of the MDR. Fig. 3(b) gives a zoom-in view of the resonance spectrum around the wavelength of 1548.326 nm, and the notch has a 3-dB bandwidth of 0.14 nm,

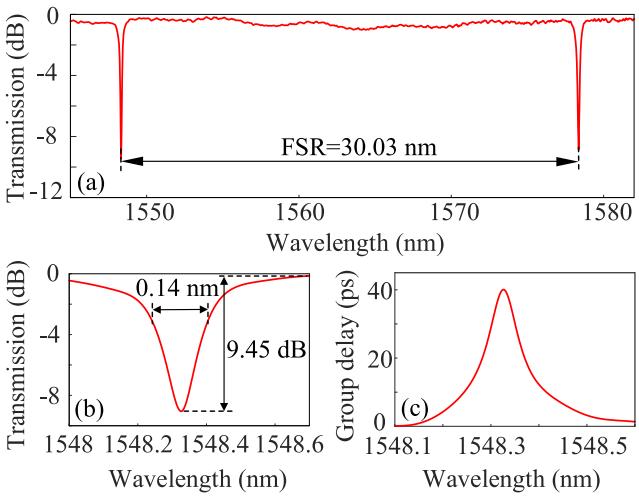

Fig. 3. (a) Measured transmission spectrum of the MDR delay element. (b) Zoom-in view of the transmission spectrum at the wavelength of 1548.326 nm. (c) Measured group delay response of the MDR delay element.

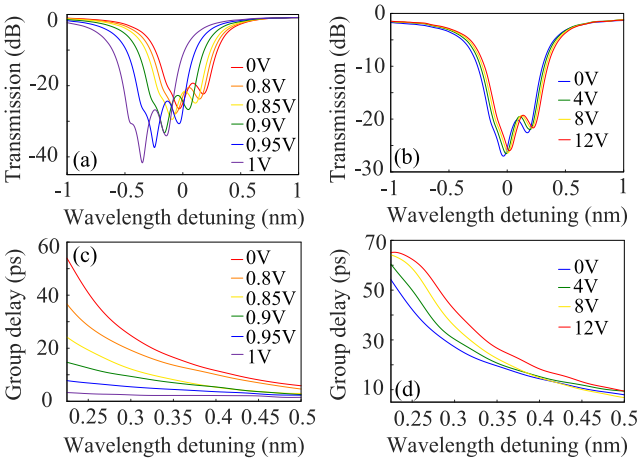

Fig. 4. (a) and (b) are the measured transmission spectra of the ODL consisting of 5 MDRs with PN junctions being forward biased and reverse biased, respectively. (c) And (d) are the measured group delay responses of the ODL consisting of 5 MDRs with PN junctions being forward biased and reverse biased, respectively.

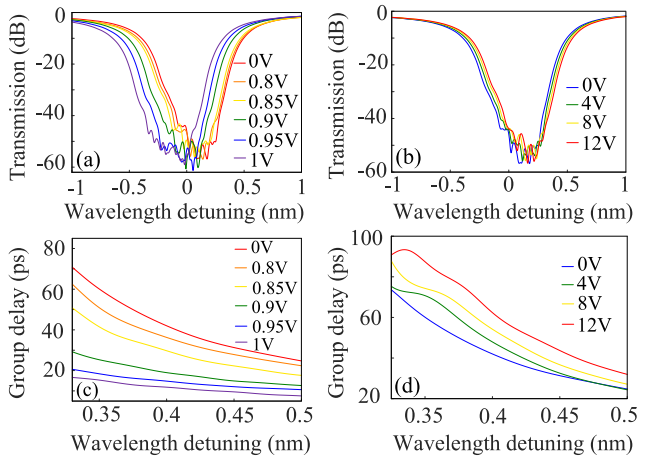

Fig. 5. (a) and (b) are the measured transmission spectra of the ODL consisting of 10 MDRs with PN junctions being forward biased and reversed biased, respectively. (c) And (d) are the measured group delay responses of the ODL consisting of 10 MDRs with PN junctions being forward biased and reversed biased, respectively.

which corresponds to a Q-factor of 11060. The extinction ratio of the notch is 9.45 dB. The measured group delay of the MDR is shown in Fig. 3(c). As can be seen, a group delay of 40 ps near the resonance wavelength can be obtained. The specially designed MDR has an ultra-compact footprint and a strong group delay, which can be used as a basic delay element in an integrated ODL.

Then, the fabricated ODL composed of 5 MDRs is characterized using the OVA. As depicted in Fig. 4(a), by applying different forward-biased voltages to the MDR, the normalized transmission spectrum of the ODL is blue shifted, which is resulted from the decrease of the effective refractive index of the waveguide induced by the free-carrier injection of the PN junction. It should be noted that the optical loss of the fabricated ODL is increased due to the additional absorption loss caused by the injected free-carriers in the PN junctions of the disks. Fig. 4(c) shows the group delay responses of the ODL under forward biased. At the wavelength detuning of 0.225 nm, the measured delay of ODL varies from 53.91 ps to 3.295 ps as the bias voltage increases from 0 V to 1 V. When the ODL is under reverse biased, the depletion regions of the PN junctions are widened due to the extraction of the free carriers. As a result, when the driven voltage is increasing, the effective refractive index of the waveguide is increased, which leads to a red-shift of the transmission spectrum of the ODL. Fig. 4(b) and (d) illustrate the transmission spectra and the group delays of the ODL under reverse biased. As the reverse-biased voltage increasing, the optical loss of ODL is reduced slightly due to the decrease of the number of free carriers in PN junctions of the disks. At the wavelength detuning of 0.225 nm, the group delay of the ODL varies from 53.91 ps to 65.08 ps when the reverse-biased voltage increases from 0 V to 12 V. The delay of the ODL is continuously tunable, which is limited only by the smallest voltage change that can be applied. The resolution of the voltage source (Keithley 2614B) used in the experiment is 500 μV within a voltage range of 20 V. The average delay tuning precision of the ODL composed of 5 MDRs is calculate to be 1.27e-05 ps and 2.33e-07 ps under forward biased and reversed biased, respectively. The loss per ps delay increment of the ODL composed of 5 MDRs is calculated to be 0.35 dB/ps and 0.36 dB/ps under forward biased and reversed biased, respectively.

The performance of the ODL composed of 10 MDRs is also evaluated. Fig. 5(a) and (c) illustrate the transmission spectra and group delay responses of the ODL under forward biased. Since the dynamic range of the OVA is only 60 dB, the deteriorated transmission of the ODL composed of 10 MDRs caused by free-carrier injection cannot be measured accurately. As the forward-biased voltage increases from 0 V to 1 V, the normalized transmission spectrum of the ODL is blue shifted and the group delay changes from 70.81 ps to 16.58 ps at the wavelength detuning of 0.33 nm. Fig. 5(b) and (d) illustrate the transmission spectra and group delay responses of the fabricated ODL under reverse biased. As the reverse-biased voltage increases from 0 V to 12 V, the normalized transmission spectrum of the ODL is red

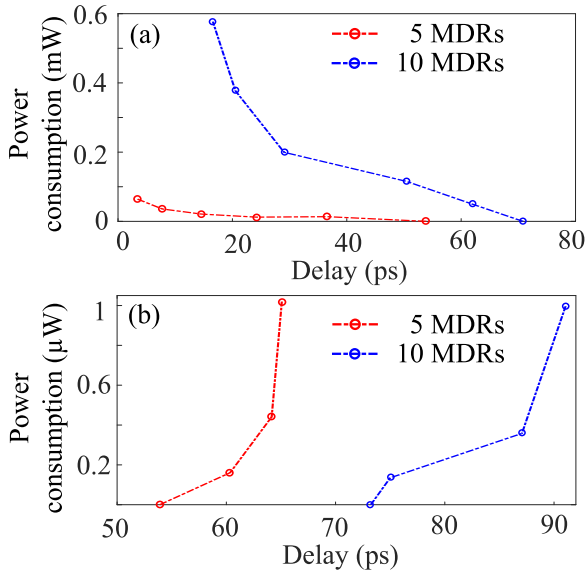

Fig. 6. Measured power consumption curves under different voltage when the PN junctions being (a) forward biased and (b) reversed biased.

shifted and the group delay of the ODL varies from 70.81 ps to 92.673 ps at the wavelength detuning of 0.33 nm. The average delay tuning precision of the ODL composed of 10 MDRs is 1.36e-05 ps and 4.55e-07 ps under forward biased and reversed biased, respectively. The loss per ps delay increment of the ODL composed of 10 MDRs is calculated to be 0.44 dB/ps under forward biased and reversed biased. To reduce the insertion loss, a balanced side-coupled integrated spaced sequence of resonator (SCISSOR) structure may be introduced into the ultra-fast tunable ODL [26], [27].

B. Power Consumption

Fig. 6 shows the measured power consumption of the ODLs. As shown in the Fig. 6(a), when the ODL composed of 5 MDRs is under forward biased, the power consumption is below 0.065 mW for a group delay ranging from 53.91 ps to 3.295 ps. When the ODL composed of 10 MDRs is under forward biased, the power consumption is below 0.58 mW for a group delay ranging from 70.81 ps to 16.58 ps. As illustrated in Fig. 6(b), when the ODL composed of 5 MDRs is under reverse biased, the power consumption is below 1.02 μW for a group delay ranging from 53.91 ps to 65.08 ps. When the ODL composed of 10 MDRs is under reverse biased, the power consumption is below 1 μW for a group delay ranging from 70.81 ps to 92.673 ps.

C. Tuning Speed

The high-speed tunability of ODL consisting of 5 MDRs is demonstrated. Fig. 7 illustrates the experimental setup for the demonstration of the rapid tunability of the ODL. The wavelength of the tunable laser source (TLS) is set to be 1548.95 nm which corresponds to a wavelength detuning of 0.256 nm. A 50 MHz electrical square-wave signal generated by an arbitrary waveform generator (AWG) is applied to the PN junction of the MDR via a high-speed radio-frequency (RF) probe. The optical

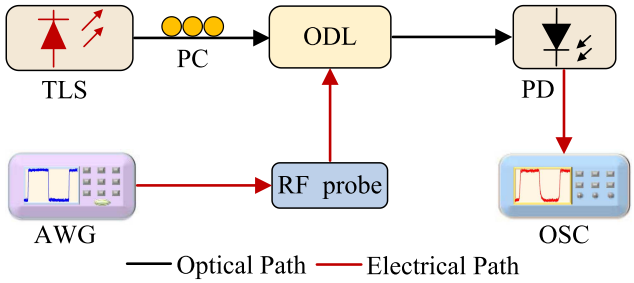

Fig. 7. Experimental setup used to measure the tuning speed of the fabricated integrated ODL.

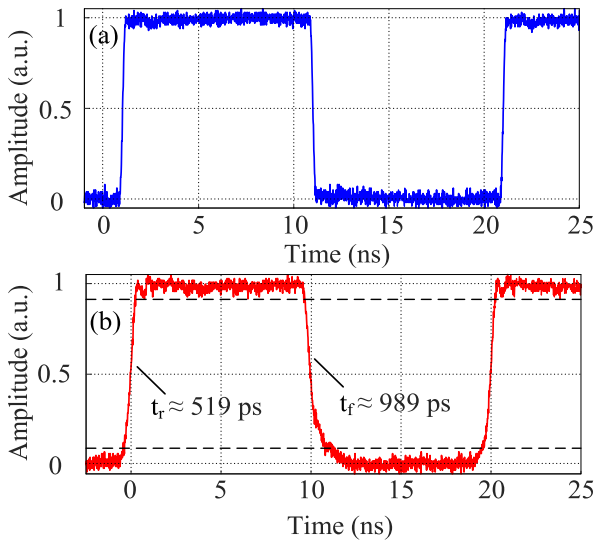

Fig. 8. Measured oscilloscope signals for the demonstration of the rapid tunability of the ODL. (a) And (b) are the square-wave electrical signal applied to the ODL and the measured variation of the optical power at the output of the ODL.

signal at the output of the ODL is sent into a photodetector (PD), and the electrical signal generated by the PD is recorded by an oscilloscope (OSC). In the experiment, the high-speed tunability of ODL is only characterized under forward biased due to the limited output voltage range of the AWG. The peak-to-peak voltage and the offset voltage of the electrical square-wave signal are set to be 800 mV and 400 mV, respectively. The response of the fabricated ODL is monitored by an OSC. Fig. 8(a) illustrates the time domain waveform of electrical square-wave signal generated by the AWG. Fig. 8(b) illustrates the measured output response of the ODL. The 10%–90% rise time and fall time of the output waveform are 519 ps and 989 ps respectively, which means that a sub-ns switching time is achieved by the proposed integrated ODL. It is noticed that the 10%–90% fall time is slower than the 10%–90% rise time. The rise time of the optical transmission is much shorter than the rise time of the charge injection and the fall time is determined by the extraction time of the carrier [39]. However, the total drift current to extract the large amount of the injected carriers is limited by the large resistance of the PN junction incorporated in the ODL.

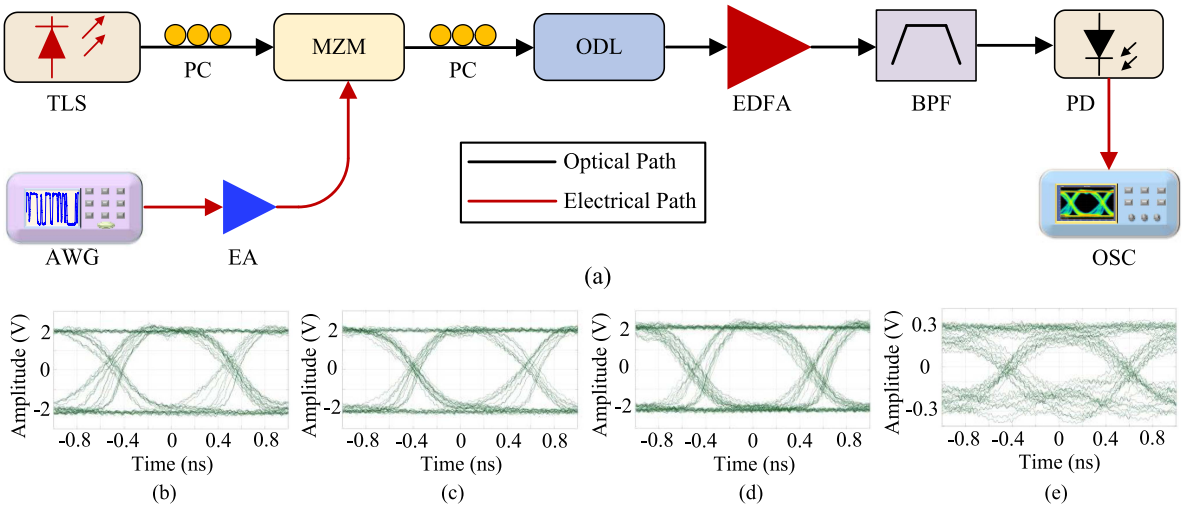

Fig. 9. (a) Experimental setup for the transmission quality of delayed optical signals through the ODL. TLS: Tunable laser source, PC: Polarization controller, MZM: Mach-Zehnder modulator, ODL: Optical delay line, EDFA: Erbium-doped fiber amplifier, BPF: Bandpass filter, PD: Photodetector, AWG: Arbitrary waveform generator, EA: Electrical amplifier, OSC: Oscilloscope. (b) (c), (d) and (e) are measured eye diagrams of 1 Gbps $2^{10}-1$ PRBS signal output from the device with (b) back-to-back (B2B) transmission, (c) no delay at off-resonance wavelength, (d) 41 ps group delay, and (e) 63 ps group delay.

TABLE I
PERFORMANCE COMPARISON OF VARIOUS INTEGRATED SOI ODLS

	Tuning scheme	Footprint (mm^2)	Delay loss (dB/ps)	Power consumption (mW)	Response time
SDL [12]	TO (TiN)	13.32	0.0995[b]	242.27	33.7 μs
SDL [13]	TO (TiN)	28.62	0.01	64 [c]	18.97 μs
SDL [14]	FCD	11.84	0.013	1384.3[c]	/
SDL [15]	FCD	/	/	/	30 ns
Grating [20]	TO (Ti)	/	0.0254	1066.7	/
Grating [21]	TO (Al)	0.015[a]	0.02	825 [c]	/
MRRs [26]	TO (Cr)	0.0075[a]	/	30	/
MRRs [27]	TO (NiCr)	/	0.06	/	< 10 μs
MRRs [28]	TO (TiN)	0.014[a]	0.06[b]	572	/
MRR [30]	FCD	/	0.42[b]	1	/
This work	FCD	0.13 (0.00917 [a])	0.44	0.58	989 ps

[a]The calculation of the footprint of the ODL does not include the electrical connections, such as metal wires and pads.
[b]The calculation of the delay loss is based on the maximum insertion loss and the maximum delay of the ODL given by the authors.
[c]The calculation of the power consumption is based on the product of the maximum delay range and the power efficiency of the ODL given by the authors.

D. Transmission Quality of Optical Signal

The quality of the optical signal transmitted through the ODL consisting of 5 MDRs is evaluated. The experimental setup is shown in Fig. 9(a). A TLS is used to generate a continuous wave optical carrier, which is launched into the Mach-Zehnder modulator (MZM) via a polarization controller (PC). A 1-Gbps NRZ OOK pseudo-random binary sequence (PRBS) signal with a length of using 2^{10}-1 is sent into the MZM. The modulated signal at the output of the MZM is launched in to the integrated ODL chip. The output signal from the chip is amplified by erbium-doped fiber amplifier (EDFA). An optical bandpass filter (BPF) is connected after the EDFA to filter out the amplified spontaneous emission (ASE) noise. The eye diagrams of the optical signal can be observed using an OSC. Fig. 9(b) shows the measured B2B eye diagram when the ODL chip is not inserted into the system. Fig. 9(c) shows the eye diagram when the ODL chip is incorporated but the optical carrier is located at the off-resonance wavelength, in which zero group delay is introduced. Fig. 9(d) and (e) show the eye diagrams with group delays of 41 ps and 63 ps. The Q factor of the eye diagrams shown in Fig. 9(c), (d) and (e) is 17.902, 15.489 and 5.455 respectively, which verifies that the proposed ODL can be used in the high-speed communication systems for precise time delay controlling.

IV. DISCUSSION AND CONCLUSION

Table I compares the performance of the proposed integrated ODL with that of the state-of-art integrated ODLs, including SWDLs [12], [13], [14], [15], waveguide Bragg grating [20], [21] and MRRs [26], [27], [28], [30]. As can be seen, the proposed integrated ODL can achieve continuous time delay tuning with an ultrahigh speed by exploiting the FCD effect on silicon. However, the proposed ultra-fast tunable ODL suffers from a large insertion loss due to the incorporation of the PN

junction. Previously, a pipin lateral diode structure has been proposed and incorporated into the optical modulator to achieve a lower insertion loss and a wide modulation bandwidth [40], [41]. Therefore, a tunable ODL with a lower insertion loss may be realized by introducing the pipin lateral diode structure into the MDR for electrical tunability.

In conclusion, an ultra-fast tunable ODL based on cascaded silicon MDRs was proposed and experimentally demonstrated. In the proposed ODL, a specially designed slab waveguide surrounding the disk was used to suppress higher-order WGMs and to support the incorporation of a lateral PN junction for electrical tunability. By exploiting the FCD effect on silicon, the time delay of the proposed ODL can be tuned with an ultrahigh speed. Multiple MDRs are connected in series to increase the time delay provided by the proposed ODL. A proof-of-concept demonstration is performed. Integrated ODLs composed of 5 and 10 MDRs are designed, fabricated, and characterized. Experimental results demonstrate that the fabricated ODL can achieve an ultra-short response time of 989 ps, a low power consumption of 0.58 mW, and a small footprint of 0.13 mm^2. The proposed ODL features ultrafast tunability, compact footprint and low power consumption, which holds potential to be widely used in next-generation phased array radar and high-speed wireless communication systems.

References

[1] J. Yao, "Microwave photonics," *J. Lightw. Technol.*, vol. 27, no. 3, pp. 314–335, Feb. 2009.

[2] J. Yao, "Photonics to the rescue: A fresh look at microwave photonic filters," *IEEE Microw. Mag.*, vol. 16, no. 8, pp. 46–60, Sep. 2015.

[3] J. T. Mok and B. J. Eggleton, "Expect more delays," *Nature*, vol. 433, pp. 811–812, 2005.

[4] D. Marpaung, J. Yao, and J. Capmany, "Integrated microwave photonics," *Nature Photon.*, vol. 13, no. 2, pp. 492–494, 2019.

[5] J. Capmany, J. Mora, I. Gasulla, J. Sancho, J. Lloret, and S. Sales, "Microwave photonic signal processing," *J. Lightw. Technol.*, vol. 31, no. 4, pp. 571–586, Feb. 2013.

[6] L. Zhang et al., "Photonic true time delay beamforming technique with ultra-fast beam scanning," *Opt. Exp.*, vol. 25, no. 13, pp. 14524–14532, 2017.

[7] Y. Liu, A. Choudhary, D. Marpaung, and B. J. Eggleton, "Gigahertz optical tuning of an on-chip radio frequency photonic delay line," *Optica*, vol. 4, no. 4, pp. 418–423, 2017.

[8] H. Shahoei and J. Yao, "Delay lines," *Wiley Encyclopedia Elect. Electron. Eng.*, pp. 1–15, 2014, doi: 10.1002/047134608X.W8234.

[9] W. Bogaerts et al., "Silicon microring resonators," *Laser Photon. Rev.*, vol. 6, no. 1, pp. 47–73, 2012.

[10] L. Zhou, X. Wang, L. Lu, and J. Chen, "Integrated optical delay lines: A review and perspective," *Chin. Opt. Lett.*, vol. 16, no. 10, 2018, Art. no. 101301.

[11] F. Yang, W. Zhang, Y. Jiang, J. Tao, and Z. He, "Highly sensitive integrated photonic sensor and interrogator using cascaded silicon microring resonators," *J. Lightw. Technol.*, vol. 40, no. 9, pp. 3055–3061, May 2022.

[12] P. Zheng et al., "A seven bit silicon optical true time delay line for Ka-band phased array antenna," *IEEE Photon. J.*, vol. 11, no. 4, Aug. 2019, Art. no. 5501809.

[13] X. Wang et al., "Continuously tunable ultra-thin silicon waveguide optical delay line," *Optica*, vol. 4, no. 5, pp. 507–515, 2017.

[14] J. Xie, L. Zhou, Z. Li, J. Wang, and J. Chen, "Seven-bit reconfigurable optical true time delay line based on silicon integration," *Opt. Exp.*, vol. 22, no. 19, pp. 22707–22715, 2014.

[15] S. Fathpour and N. A. Riza, "Silicon-photonics-based wideband radar beamforming: Basic design," *Opt. Eng.*, vol. 49, no. 1, pp. 1–7, 2010.

[16] C. Zhu et al., "Silicon integrated microwave photonic beamformer," *Optica*, vol. 7, no. 9, pp. 1162–1170, 2020.

[17] S. Idres and H. Hashemi, "Optical binary switched delay line based on low loss multimode waveguide," in *Proc. Opt. Fiber Commun. Conf. Exhib.*, 2022, pp. 1–3.

[18] H. Sun, Y. Wang, and L. R. Chen, "Integrated discretely tunable optical delay line based on step-chirped subwavelength grating waveguide Bragg gratings," *J. Lightw. Technol.*, vol. 38, no. 19, pp. 5551–5560, Oct. 2020.

[19] I. Giuntoni et al., "Continuously tunable delay line based on SOI tapered Bragg gratings," *Opt. Exp.*, vol. 20, no. 10, pp. 11241–11246, 2012.

[20] X. Wang, Y. Zhao, Y. Ding, S. Xiao, and J. Dong, "Tunable optical delay line based on integrated grating-assisted contradirectional couplers," *Photon. Res.*, vol. 6, no. 9, pp. 880–886, 2018.

[21] W. Shi, V. Veerasubramanian, D. Patel, and D. V. Plant, "Tunable nanophotonic delay lines using linearly chirped contradirectional couplers with uniform Bragg gratings," *Opt. Lett.*, vol. 39, no. 3, pp. 701–703, 2014.

[22] S. Khan and S. Fathpour, "Complementary apodized grating waveguides for tunable optical delay lines," *Opt. Exp.*, vol. 20, no. 18, pp. 19859–19867, 2012.

[23] J. Wang et al., "Subwavelength grating enabled on-chip ultra-compact optical true time delay line," *Sci. Rep.*, vol. 6, no. 1, 2016, Art. no. 30235.

[24] F. Xia, L. Sekaric, and Y. Vlasov, "Ultracompact optical buffers on a silicon chip," *Nature Photon.*, vol. 1, no. 1, pp. 65–71, 2007.

[25] M. L. Cooper et al., "235-ring coupled-resonator optical waveguides," in *Proc. Conf. Lasers Electro-Opt.*, 2010, Paper CTuHH3.

[26] J. Cardenas et al., "Wide-bandwidth continuously tunable optical delay line using silicon microring resonators," *Opt. Exp.*, vol. 18, no. 25, pp. 26525–26534, 2010.

[27] P. A. Morton, J. Cardenas, J. B. Khurgin, and M. Lipson, "Fast thermal switching of wideband optical delay line with no long-term transient," *IEEE Photon. Technol. Lett.*, vol. 24, no. 6, pp. 512–514, Mar. 2012.

[28] F. Shinobu, N. Ishikura, Y. Arita, T. Tamanuki, and T. Baba, "Continuously tunable slow-light device consisting of heater-controlled silicon microring array," *Opt. Exp.*, vol. 19, no. 14, pp. 13557–13564, 2011.

[29] J. Xie, L. Zhou, Z. Zou, J. Wang, X. Li, and J. Chen, "Continuously tunable reflective-type optical delay lines using microring resonators," *Opt. Exp.*, vol. 22, no. 1, pp. 817–823, 2014.

[30] X. Luo, H. Chen, and A. W. Poon, "Electro-optical tunable time delay and advance in silicon microring resonators," *Opt. Lett.*, vol. 35, no. 17, pp. 2940–2942, 2010.

[31] S. Feng, X. Luo, S. Du, and A. W. Poon, "Electro-optical tunable time delay and advance in a silicon feedback-microring resonator," *Opt. Lett.*, vol. 36, no. 7, pp. 1278–1280, 2011.

[32] M.-A. Bianki, C. Lemieux-Leduc, R. Guertin, and Y.-A. Peter, "Mutlilayer wedge disks CROW for an optical delay line," *J. Lightw. Technol.*, vol. 40, no. 3, pp. 770–775, Feb. 2022.

[33] Q. Huang, G. Song, J. Chen, Z. Shu, and J. Yu, "Proposal and fabrication of an electrooptically controlled multimode microresonator for continuous fast-to-slow light tuning," *IEEE Photon. J.*, vol. 6, no. 4, Aug. 2014, Art. no. 2201011.

[34] Q. Li, A. A. Eftekhar, P. Alipour, A. H. Atabaki, S. Yegnanarayanan, and A. Adibi, "Low-loss microdisk-based delay lines for narrowband optical filters," *IEEE Photon. Technol. Lett.*, vol. 24, no. 15, pp. 1276–1278, Aug. 2012.

[35] S. Nishikawa, S. Lan, N. Ikeda, Y. Sugimoto, H. Ishikawa, and K. Asakawa, "Optical characterization of photonic crystal delay lines based on one-dimensional coupled defects," *Opt. Lett.*, vol. 27, no. 23, pp. 2079–2081, 2002.

[36] S. Elshahat, I. Abood, K. Khan, A. Yadav, L. Bibbò, and Z. Ouyang, "Five-line photonic crystal waveguide for optical buffering and data interconnection of picosecond pulse," *J. Lightw. Technol.*, vol. 37, no. 3, pp. 788–798, Feb. 2019.

[37] S. Romero-García et al., "High-speed resonantly enhanced silicon photonics modulator with a large operating temperature range," *Opt. Lett.*, vol. 42, no. 1, pp. 81–84, 2017.

[38] D. K. Gifford, B. J. Soller, M. S. Wolfe, and M. E. Froggatt, "Optical vector network analyzer for single-scan measurements of loss, group delay, and polarization mode dispersion," *Appl. Opt.*, vol. 44, no. 34, pp. 7282–7286, 2005.

[39] Q. Xu, S. Manipatruni, B. Schmidt, J. Shakya, and M. Lipson, "12.5 Gbit/s carrier-injection-based silicon micro-ring silicon modulators," *Opt. Exp.*, vol. 15, no. 2, pp. 430–436, 2007.

[40] G. Rasigade, D. Marris-Morini, L. Vivien, and E. Cassan, "Performance evolutions of carrier depletion silicon optical modulators: From PN to PIPIN diodes," *IEEE J. Sel. Topics Quantum Electron.*, vol. 16, no. 1, pp. 179–184, Jan./Feb. 2010.

[41] M. Ziebell et al., "40 Gbit/s low-loss silicon optical modulator based on a pipin diode," *Opt. Exp.*, vol. 20, no. 10, pp. 10591–10596, 2012.